Available online at www.sciencedirect.com
SCIENCE DIRECT®
ELSEVIER
European Journal of Mechanics B/Fluids 22 (2003) 411–430
EUROPEAN JOURNAL OF MECHANICS B/FLUIDS

Modal growth and non-modal growth in a stretched shear layer

Stéphane Le Dizès

Institut de recherche sur les phénomènes hors équilibre, 49, rue F. Joliot-Curie, BP 146, 13384 Marseille cedex 13, France

Received 12 February 2003; received in revised form 20 June 2003; accepted 7 July 2003

Abstract

The evolution of two-dimensional linear perturbations in a uniform shear layer stretched along the streamwise direction is considered in this work. The velocity field of the basic flow is assumed to be given by the following exact solution of Navier–Stokes equations $\mathbf{U} = (\gamma x + (1/S(t))\,\mathrm{erf}(y/a(t)), -\gamma y, 0)$ where erf is the error function, $a(t)$ and $S(t)$ are time-varying functions. The solution is governed by two parameters: the Reynolds number *Re* and the stretching rate γ (non-dimensionalized by the initial maximum vorticity) which is assumed to be a positive constant. Using a direct-adjoint technique, perturbations which maximize the energy gain during a time interval $(0, t_f)$ are computed for various t_f, γ and *Re*. For each case, the results are compared with those obtained by considering a single local normal mode (WKBJ approach). For small t_f ($t_f < 10$) and large Reynolds numbers, transient effects associated with non-modal growth are clearly visible: they favor large wavenumbers which are locally stable. However, they are found not to provide important energy gains. Moreover, transient growth is shown not to be significantly affected by stretching and to diminish with viscosity. For larger t_f ($t_f > 20$), instability takes over transients: the WKBJ approximation is shown to provide a good estimate of the maximum gain whatever the Reynolds number (>10) and the stretching rate (<0.025). However, differences concerning the most amplified wavenumbers remain visible and increase with γ. For very large times, stretching moves the local wavenumber toward zero. A non-viscous asymptotic study performed for small k shows that although the perturbation energy ultimately diminishes, it decreases less rapidly than the basic flow energy density. Stretching therefore never stabilizes the shear layer for large Reynolds numbers. The results obtained in the WKBJ framework are also extended to more general configurations including three-dimensional perturbations and triaxial stretching fields.

1. Introduction

A vortex sheet during its roll-up or the braid region between two adjacent vortices in a shear flow are typical examples of longitudinally stretched shear layers. The goal of this article is to understand how stretching and viscosity affect, in such a flow, transient growth and modal growth associated with the Kelvin–Helmholtz instability.

A shear layer is the flow between two uniform streams. Since the works of Kelvin, Helmholtz and Rayleigh, this flow has been known to be unstable with respect to small disturbances. Rayleigh [1] (see also for instance Drazin and Reid [2]) proved the non-viscous character of the instability and showed that the presence of inflexion point in the velocity profile was necessary for instability. Esch [3], Tatsumi and Gotoh [4] and Betchov and Szewczyk [5] analysed the effect of viscosity and demonstrated that the instability extended down to zero Reynolds number. Numerous results obtained with a parallel flow assumption have also been applied with more or less success to spatially developing shear flows (see, for instance, Ho and Huerre [6] for a review). For these flows however, Huerre and Monkewitz [7] have shown that the temporal stability analysis must be replaced by a spatial stability analysis. The weakly diffusing character of the shear layer is usually taken into account by using a WKBJ approximation ansatz. In this approach, the perturbation is assumed to be a local plane wave with the same stability properties

E-mail address: ledizes@irphe.univ-mrs.fr (S. Le Dizès).

0997-7546/$ – see front matter
doi:10.1016/S0997-7546(03)00057-8

of a wave on a parallel and time-invariant shear layer. The basic assumption of this approach is a scale separation, that is both space and time variation scales of the shear layer are very large compared to typical wavelengths and time periods of instability waves. There is another intrinsic limitation. As the perturbation is assumed to be a single local plane wave, the WKBJ approach cannot capture algebraic growth associated with a decomposition on several non-orthogonal waves. This limitation is important in linearly stable flows such as plane Couette flows as no growth is obtained in the WKBJ framework although enormous energy gains are possible (Trefethen et al. [8], Butler and Farrell [9]). For an unstable mixing layer, we shall see that the WKBJ approach also underestimates the maximum energy gain for small times but that the differences become relatively weak for large times.

In the present work, we consider, as basic flow, a uniform time-dependent shear layer. The time-dependency is induced by viscous diffusion and a uniform stretching field which elongates the shear layer along the streamwise direction. Various Reynolds numbers and stretching rates are considered. Our goal is to perform a generalized stability analysis (Farrell and Ioannou [10], see also Schmid and Henningson [11]) of this flow by computing optimal perturbations. There are two motivations. First, we want to determine whether important transient growth can exist in a stretched and viscous shear layer. Second, we wish to analyse the effects of stretching and viscosity on the transient and instability growth in order to validate a method that could be used to compute energy gain estimates in more complex configurations.

Most studies have considered shear layers which are stretched in the spanwise direction (i.e., along with the vorticity direction). Lin and Corcos [12] and Neu [13] were motivated by providing nonlinear scenarios for the collapse of such layers. Beronov and Kida [14] analysed the two-dimensional stability of the Burgers layer which is an exact stationary solution. They did not consider transient effects but showed that the stretching field modifies the characteristics of the normal modes and makes the shear layer stable below $Re = 1$. Gomez and Rossi [15] recently examined transient growth in a discontinuous model of shear layer stretched along the spanwise direction. They demonstrated by a semi-analytical approach how spanwise stretching amplifies the growth of the perturbations.

The effect of longitudinal stretching was considered only in the framework of infinitely thin non-viscous shear layer (vortex sheet). Moore and Griffith-Jones [16] showed how stretching modifies the growth of the Kelvin Helmholtz instability by considering an expanding circular vortex sheet. Moore [17] extended the analysis to more general vortex sheet and discussed the validity of the local approximation when the strength of the sheet is not uniform. Although these analyses do not consider the finite size of the shear layer nor viscous effects, they are connected to our study when small wavenumbers and large Reynolds numbers are considered (see Section 4.3 and Appendix).

The paper is organized as follows. In Section 2.1, the stretched shear layer model is presented and the perturbation equations are derived. Both the optimization procedure and the WKBJ approach are described in this section. For the optimization procedure, we use a similar iteration technique as in Luchini and Bottaro [18] and Andersson et al. [19] to compute the optimal energy perturbations. It is based on multiple integrations of the direct perturbation equations and of the adjoint equations. The results are presented in Sections 3 and 4. The case of an unstretched diffusing shear layer is considered first. Both transient and viscous effects are identified in this section. The results are compared to early computations by Betchov and Szewczyk [5]. Stretching effects are analysed in details in Section 4. The characteristics of the optimal energy perturbation are compared to most amplified WKBJ waves for various stretching rates, Reynolds numbers and final optimization times. The results of an asymptotic study, performed in appendix, applicable for large t_f and large Reynolds numbers are discussed in Section 4.3. It is shown that stretching does not stabilize the shear layer. In the final section (Section 5), the results are summarized. Three-dimensional effects are also considered in this section. The growth of three-dimensional perturbations on a viscous shear layer subjected to a triaxial stretching field is examined in the WKBJ framework.

2. Basic flow and perturbation definitions

2.1. Basic flow

The 2D dynamics of a shear layer is governed by the vorticity equation:

$$\frac{\partial \omega}{\partial t} + (\mathbf{U} \cdot \nabla)\omega = \nu \Delta \omega, \tag{1}$$

where ν is the kinematic viscosity. The velocity $\mathbf{U} = (U_x, U_y)$ and the vorticity ω are connected to the streamfunction ψ through the usual relations:

$$U_x = \frac{\partial \psi}{\partial y}, \qquad U_y = -\frac{\partial \psi}{\partial x}, \qquad \omega = -\Delta \psi.$$

Here, in most of the paper, we consider a shear layer which is uniformly stretched along the streamwise direction and which possesses a velocity field of the form:

$$(U_x, U_y) = \big(U_0(y,t) + \gamma x, -\gamma y\big), \tag{2}$$

where γ is the strain rate of the stretching field. In expression (2), it is implicitly assumed that γ is independent of spatial variables. It may however depend on time. When γ is positive, the shear layer is stretched. When it is negative, it is compressed. The vorticity field $\omega_0 = \omega_0(y,t)$ associated with (2) satisfies

$$\frac{\partial \omega_0}{\partial t} - \gamma y \frac{\partial \omega_0}{\partial y} = \nu \frac{\partial^2 \omega_0}{\partial y^2}. \tag{3}$$

The following change of variables

$$\bar{y} = S(t)y, \quad \bar{t} = \int_0^t S^2(r)\,\mathrm{d}r,$$

with

$$S(t) = \exp\left(\int_0^t \gamma(r)\,\mathrm{d}r\right), \tag{4}$$

transforms (3) into a simple diffusion equation

$$\frac{\partial \omega_0}{\partial \bar{t}} = \nu \frac{\partial^2 \omega_0}{\partial \bar{y}^2}, \tag{5}$$

which can be integrated without difficulty from any initial condition.

In the following, we focus on the shear layer which corresponds to the self-similar profile:

$$\omega_0(\bar{y}, \bar{t}) = -\frac{1}{\bar{a}}\,\mathrm{e}^{-(\bar{y}/\bar{a})^2}, \tag{6}$$

with $\bar{a}(\bar{t}) = \sqrt{1 + 4\nu\bar{t}}$. With respect to the initial variables, the vorticity then reads

$$\omega_0(y,t) = -\frac{1}{S(t)a(t)}\,\mathrm{e}^{-(y/a(t))^2}, \tag{7}$$

where $S(t)$ is given by (4) and $a(t)$ by

$$a(t) = \frac{\sqrt{1 + 4\nu \int_0^t S^2}}{S(t)}. \tag{8}$$

The streamwise velocity associated with (6) is

$$U_0 = \frac{1}{S}\,\mathrm{erf}\left(\frac{\bar{y}}{\bar{a}}\right) = \frac{1}{S}\,\mathrm{erf}\left(\frac{y}{a}\right). \tag{9}$$

In (7) and (9), the initial values of the velocity difference $\delta U_0 = (U_0(+\infty) - U_0(-\infty))/2$ and of the shear layer width are unitary, which implicitly assumes that these two quantities have been used to non-dimensionalize time and space variables. In particular, this means that ν in (8) is the inverse of the initial Reynolds number Re_i defined by

$$Re_i = \frac{\delta U_0(0) a(0)}{\nu} = \frac{1}{\nu}. \tag{10}$$

Although the analysis can be carried out for any varying γ, we shall mostly consider in the present paper a positive and constant stretching rate $\gamma = \gamma_0 > 0$. In that case, one has

$$\bar{y} = \exp(\gamma t)y, \qquad \bar{t} = \frac{\exp(2\gamma t) - 1}{2\gamma}.$$

Thus, the large-time vorticity field of the shear layer is in the unstretched variables of the form:

$$\omega_0(y,t) \sim \frac{\gamma}{2\nu \exp(2\gamma t)} \exp\left(-\frac{\gamma y^2}{2\nu}\right). \tag{11}$$

Expression (11) demonstrates that the vorticity magnitude within the shear layer decreases exponentially due to the stretching field. This effect can be easily understood by modelling the shear layer by an array of point vortices, as it is done in the so called "vortex method" (e.g., Cottet and Koumoutsakos [20]). Indeed, as stretching increases the separation distance between point vortices, the vortex density which is a measure of the vorticity magnitude decreases. Note, however, that the width of the shear layer converges to a finite value $a_\infty = \sqrt{2\nu/\gamma}$ for large times. This value corresponds to an equilibrium point between two opposite effects: viscosity which tends to enlarge the shear and transverse compression (or longitudinal stretching) which tends to concentrate it.

It is important to point out that the solution (6) differs from the so-called Burgers layer (see, for instance, Batchelor [21]). In Burgers layer, the stretching direction is perpendicular to the streamwise velocity and aligned along with the vorticity direction. Vorticity is thus enhanced by stretching which compensates viscous diffusion. Burgers layer is a fully steady solution. The two-dimensional stability of Burgers layer has been considered by Beronov and Kida [14]. Beronov [22] extended Burgers layer solution by providing all the steady shear layer solutions in a triaxial strain field. He also extended the above time-dependent self-similar solution to a triaxial strain field configuration. The stability of these more general solutions are briefly discussed in Section 5.

The main goal of the paper is to analyse the dynamics of linear perturbations to the basic flow (6).

2.2. Perturbation equations

The equations satisfied by 2D linear disturbances are obtained by linearizing equation (1) around the basic flow defined by (2) and (9). The equations for the perturbation vorticity ω and streamfunction are

$$\frac{\partial\omega}{\partial t} + \big(U_0(y,t) + \gamma x\big)\frac{\partial\omega}{\partial x} - \gamma y\frac{\partial\omega}{\partial y} + U_{0yy}(y,t)\frac{\partial\psi}{\partial x} = \nu\Delta\omega, \tag{12a}$$

$$\omega = -\Delta\psi. \tag{12b}$$

As above, it is convenient to eliminate the stretching terms $\gamma x\partial/\partial x$ and $-\gamma y\partial/\partial y$ using the following change of variables:

$$\bar{x} = \frac{x}{S(t)}, \qquad \bar{y} = S(t)y, \tag{13}$$

with $S(t) = \exp(\int_0^t \gamma(r)\,\mathrm{d}r)$, such that Eqs. (12a,b) become

$$\frac{\partial\omega}{\partial t} + \frac{\overline{U}_0}{S^2}\frac{\partial\omega}{\partial\bar{x}} + \overline{U}_{0\bar{y}\bar{y}}\frac{\partial\psi}{\partial\bar{x}} = \nu\left[\frac{1}{S^2}\frac{\partial^2}{\partial\bar{x}^2} + S^2\frac{\partial^2}{\partial\bar{y}^2}\right]\omega, \tag{14a}$$

$$\omega = -\left[\frac{1}{S^2}\frac{\partial^2}{\partial\bar{x}^2} + S^2\frac{\partial^2}{\partial\bar{y}^2}\right]\psi, \tag{14b}$$

where

$$\overline{U}_0(\bar{y},t) = S(t)U_0 = \operatorname{erf}\left(\frac{\bar{y}}{\bar{a}}\right), \tag{15a}$$

$$\overline{U}_{0\bar{y}\bar{y}}(\bar{y},t) = \frac{1}{S}\frac{\partial^2 U_0}{\partial y^2} = -2\frac{\bar{y}}{\bar{a}^3}\,\mathrm{e}^{-(\bar{y}/\bar{a})^2}. \tag{15b}$$

Eqs. (14a,b) are homogeneous with respect to $\bar{x}$ which allows a spectral decomposition of the form

$$(\omega,\psi) = \big(\omega_\kappa(\bar{y},t),\psi_\kappa(\bar{y},t)\big)\,\mathrm{e}^{\mathrm{i}\kappa\bar{x}}. \tag{16}$$

The equations for ω_κ and ψ_κ, obtained by substituting (16) in (14) read:

$$\frac{\partial\omega_\kappa}{\partial t} + \frac{\mathrm{i}\kappa\overline{U}_0}{S^2}\omega_\kappa + \mathrm{i}\kappa\overline{U}_{0\bar{y}\bar{y}}\psi_\kappa = \nu\left[S^2\frac{\partial^2}{\partial\bar{y}^2} - \frac{\kappa^2}{S^2}\right]\omega_\kappa, \tag{17a}$$

$$\omega_\kappa = \left[\frac{\kappa^2}{S^2} - S^2\frac{\partial^2}{\partial\bar{y}^2}\right]\psi_\kappa = -\Delta_\kappa(t)\psi_\kappa. \tag{17b}$$

Note that these equations contain explicit time-dependency through both $S(t)$ and $\bar{a}(t)$.

2.3. Generalized stability analysis

2.3.1. Energy gain

Classical stability analysis is not possible as both the behavior of the perturbations and of the basic flow depend on time. Stability characteristics are therefore not associated with the growth rate of the perturbation as the latter quantity is not defined or varies in time. Instead of growth rates, one must consider the relative gain in amplitude that the perturbation can reach during a given time interval. Optimal perturbations are by definition the perturbations which maximize such a gain. They naturally depend on the quantity chosen for the optimization. In the present paper, we shall consider the energy. This is the usual choice. We shall not try to demonstrate that it necessarily constitutes the most relevant choice.

The definition of the relative energy gain is not straightforward in the present case as the basic flow energy is infinite. Several choices have been made in the literature. Often, the basic flow energy is simply ignored. This can be justified when it does not vary. Here, as seen on expression (9), the maximum basic flow velocity varies as $1/S$, so one can expect, in presence of stretching, important variations of the basic flow energy in any finite volume. In order to account for these energy variations, we shall consider a finite volume of fluid, and then look whether a consistent definition can be obtained when the volume goes to infinity. It is also natural to consider a volume of fluid which is stretched in time. In such a way, the effect of the stretching field is taken into account without having to deal with the unbounded character if its velocity field. So, let us consider the energy E of the velocity field (U_x, U_y) in a fixed volume $V = [-A, A] \times [-B, B]$ of the stretched variables $(\bar{x}, \bar{y})$:

$$E(t) = \frac{1}{2} \iint_V \left(|U_x|^2 + |U_y|^2 \right) \mathrm{d}\bar{x}\, \mathrm{d}\bar{y}. \tag{18}$$

With this definition, the basic flow energy is defined by

$$E_0(t) = \frac{1}{2} \iint_V |U_0|^2 \, \mathrm{d}\bar{x}\, \mathrm{d}\bar{y} = \frac{A}{S^2} \int_{-B}^{B} \mathrm{erf}^2\left(\frac{\bar{y}}{\bar{a}} \right) \mathrm{d}\bar{y}, \tag{19}$$

which becomes, for large values of B,

$$E_0(t) \sim \frac{2AB}{S^2(t)}. \tag{20}$$

For a perturbation mode of initial wavenumber κ, the energy is given by

$$E_\kappa(t) = \frac{1}{2} \iint_V \left(|u_\kappa|^2 + |v_\kappa|^2 \right) \mathrm{d}\bar{x}\, \mathrm{d}\bar{y} = A \int_{-B}^{B} \left(|u_\kappa|^2 + |v_\kappa|^2 \right) \mathrm{d}\bar{y}, \tag{21}$$

which reads, for large B (if ones assumes that the perturbation is localized)

$$E_\kappa(t) \sim A \int_{-\infty}^{+\infty} \psi_\kappa^* \omega_\kappa \, \mathrm{d}\bar{y}, \tag{22}$$

where the star denotes the complex conjugate.

The important point is that for large B, the relative gain of energy between the instants 0 and t becomes independent of A and B. Its expression is given by

$$G_\kappa(t) = \lim_{B \to \infty} \frac{E_\kappa(t)/E_0(t)}{E_\kappa(0)/E_0(0)} = S^2(t) \frac{\int_{-\infty}^{+\infty} \psi_\kappa^*(t) \omega_\kappa(t) \, \mathrm{d}\bar{y}}{\int_{-\infty}^{+\infty} \psi_\kappa^*(0) \omega_\kappa(0) \, \mathrm{d}\bar{y}}. \tag{23}$$

We shall use this definition of the energy gain in the rest of the paper. The $S^2(t)$ factor in the above expression is associated with the evolution of the basic flow characteristics. Note that this factor is in agreement with the evolution of maximum basic flow velocity in $1/S$ as mentioned above. As it will be seen in Section 4, it may significantly affect the evolution of the energy gain $G_\kappa(t)$.

2.3.2. Optimal perturbations

Optimal energy perturbations are, as mentioned above, perturbations which maximize the energy gain $G_\kappa(t)$. If one introduces the scalar product

$$\langle f | g \rangle_{\{\kappa,t\}} = - \int_{-\infty}^{+\infty} f^* \Delta_\kappa(t) g \, \mathrm{d}\bar{y}, \tag{24}$$

the expression for the energy gain can be written as

$$G_\kappa(t) = S^2(t)\frac{\|\psi_\kappa(t)\|^2_{\{\kappa,t\}}}{\|\psi_\kappa(0)\|^2_{\{\kappa,0\}}}. \tag{25}$$

Note that the scalar product depends on both κ and t via the operator $\Delta_\kappa(t)$ defined in (17b). In order to simplify the notation, these dependencies will be omitted from the scalar product parameters in the rest of the paper.

The maximum energy gain of the perturbations of initial wavenumber κ between the instants $t=0$ and $t=t_f$ is defined by

$$G^{\max}_\kappa(t_f) = \max_{\|\psi_\kappa(0)\|=1}\left(\left\|\psi_\kappa(t_f)\right\|^2\right). \tag{26}$$

If one defines the evolution operator

$$\mathcal{L}_{\{\kappa,t_f\}} : \psi_\kappa(0) \mapsto \psi_\kappa(t_f), \tag{27}$$

one can write

$$\|\psi_\kappa\|^2 = \left\langle \mathcal{L}_{\{\kappa,t_f\}}\left(\psi_\kappa(0)\right) | \mathcal{L}_{\{\kappa,t_f\}}\left(\psi_\kappa(0)\right)\right\rangle = \left\langle \mathcal{L}^A_{\{\kappa,t_f\}} \circ \mathcal{L}_{\{\kappa,t_f\}}\left(\psi_\kappa(0)\right) | \psi_\kappa(0)\right\rangle, \tag{28}$$

where $\mathcal{L}^A_{\{\kappa,t_f\}}$ is the adjoint operator of $\mathcal{L}_{\{\kappa,t_f\}}$ associated with the scalar product $\langle f|g\rangle$.

Expression (28) for $\|\psi_\kappa\|^2$ allows another definition for the maximum energy growth: $G^{\max}_\kappa(t_f)$ is the largest eigenvalue of the symmetric operator $\mathcal{L}^A_{\{\kappa,t_f\}} \circ \mathcal{L}_{\{\kappa,t_f\}}$, the optimal perturbation $\psi^{\max}_\kappa$ being the associated eigenmode. Computationally, this definition is more convenient. Indeed, if one assumes that the largest eigenvalue is simple and well-separated (i.e., not an accumulation point of the spectrum), the functions defined by power iterations

$$\psi^{(n+1)} = \mathcal{L}^A_{\{\kappa,t_f\}} \circ \mathcal{L}_{\{\kappa,t_f\}}\left[\psi^{(n)}\right], \tag{29}$$

converge towards $\psi^{\max}_\kappa$ if the initial condition $\psi^{(0)}$ is not orthogonal to $\psi^{\max}_\kappa$. In practice, it turns out that the non-orthogonality condition is not a problem and that five iterations are often more than enough for convergence. More details on this direct-adjoint technique can be found in Andersson et al. [19].

The numerical integration of the direct and adjoint equations is carried out using a Chebichev collocation technique together with the mapping $Y = y/\sqrt{y^2+L^2}$ for the spatial variable, and a second order Adams–Bashforth scheme for the time variable. In most simulations, we use 65 Chebichev polynomials with $L=2$ in the mapping. As demonstrated in Melcalfe et al. [23], this is more than enough for the description of the 2D linear dynamics. The code is written with Matlab© and uses the differential Matrix package developed by Weideman and Reddy [24].

2.3.3. WKBJ perturbations

When $\gamma \ll 1$ and $Re \gg 1$, the time-dependency is weak: the perturbation can be searched under the form of a local normal mode (WKBJ approach)

$$\psi_\kappa = \tilde{\psi}_\kappa \exp\left(\int_0^t \sigma(s)\,\mathrm{d}s\right). \tag{30}$$

The amplitude $\tilde{\psi}_\kappa$ and the local growth rate σ thus satisfy, at leading order, the Orr–Sommerfeld equation

$$(\tilde{\sigma} + \mathrm{i}k\widetilde{U}_0)\left[\frac{\partial^2}{\partial\tilde{y}^2} - k^2\right]\tilde{\psi}_\kappa - \mathrm{i}k\widetilde{U}_{0\tilde{y}\tilde{y}}\tilde{\psi}_\kappa = \frac{1}{Re}\left[\frac{\partial^2}{\partial\tilde{y}^2} - k^2\right]^2\tilde{\psi}_\kappa, \tag{31}$$

where

$$\begin{aligned}
&\tilde{y} = \frac{y}{a(t)} = \frac{\bar{y}}{\bar{a}},\\
&\widetilde{U}_0(\tilde{y}) = \mathrm{erf}(\tilde{y}),\\
&k = \frac{\kappa a(t)}{S(t)} = \frac{\kappa\bar{a}}{S^2},\\
&Re = a(t)/\nu/S(t) = \bar{a}/S^2/\nu,\\
&\tilde{\sigma} = \sigma a(t)S(t) = \sigma\bar{a}(t).
\end{aligned} \tag{32}$$

At leading order, the local growth rate $\tilde{\sigma}$ is then connected through k and Re by the (Orr–Sommerfeld) dispersion relation $\tilde{\sigma} = \sigma_{\mathrm{erf}}[k, Re]$ associated with the "erf" velocity profile. In other words, we have the relation

$$\sigma = \frac{1}{a(t)S(t)}\sigma_{\mathrm{erf}}\left[\kappa\frac{a(t)}{S(t)}, \frac{a(t)}{\nu S(t)}\right]. \tag{33}$$

In the WKBJ framework, the function $\tilde{\psi}_\kappa$ is written as $\tilde{\psi}_\kappa = \tilde{\phi}(\tilde{y}, k, Re)F(t, k, Re)$ where $F(t, k, Re)$ is an amplitude slowly varying with respect to the time variable. It follows that the perturbation vorticity reads

$$\omega_\kappa = \widetilde{\omega}(\tilde{y}, k, Re)\frac{F(t, k, Re)}{a^2(t)}\exp\left(\int_0^t \sigma(s)\,\mathrm{d}s\right). \tag{34}$$

If the amplitude $F(t, k, Re)$ is conveniently chosen such that $\int_{-\infty}^{+\infty}\tilde{\phi}^*\widetilde{\omega}\,\mathrm{d}\tilde{y} = 1$, an estimate for the energy gain (25) is provided by

$$G_\kappa^{\mathrm{WKBJ}}(t) = C^{\mathrm{WKBJ}}(t, k, Re)\frac{S^3(t)}{a(t)}\exp\left(2\int_0^t \sigma(s)\,\mathrm{d}s\right), \tag{35}$$

where $C^{\mathrm{WKBJ}}(t, k, Re) = |F(t, k, Re)|^2$.

The function $C^{\mathrm{WKBJ}}(t, k, Re)$ varies on the same slow time scale as $S(t)$ and $a(t)$, and satisfies $C^{\mathrm{WKBJ}}(0, \kappa, Re) = 1$. Although C^{WKBJ} can be computed for fixed parameters by classical techniques (Van Dyke [25]), no explicit expression is available in terms of k or Re. In order to get an explicit formula, we therefore postulate that $C^{\mathrm{WKBJ}} = 1$ in the above expression. This will define what we shall call in the rest of the paper, the WKBJ estimate. This assumption is a priori justified only if $S(t)$ and $a(t)$ are close to 1. However, as it will be shown below, the WKBJ estimate will also provide a fairly good estimate for moderate values of S and a. In Section 4.3, the non-viscous small wavenumber limit will be studied. It will permit to show that $C^{\mathrm{WKBJ}}(t, k, \infty)$ varies as $1/S^2$ when $k \to 0$.

2.4. The characteristic parameters and the kinematic effect of stretching and viscosity

Before starting the analysis, it is important to define a few important physical quantities that will be useful to describe the characteristics of the perturbations. Moreover, simple kinematic effects can readily be extracted from the above analysis.

As explained in the previous section, the optimization procedure and the WKBJ analysis provide the optimal gain $G_\kappa^{\max}$ and the WKBJ estimate G_κ^{WKBJ} for each value of the (initial) Reynolds number Re_i, of the (initial) wavenumber κ, of the stretching rate γ and of the final time t_f. For comparison with normal mode growth rate, it will be useful to also define the mean growth rate associated with those gains:

$$\sigma_\kappa^{\max}(t_f) = \frac{\ln(G_\kappa^{\max}(t_f))}{t_f}, \qquad \sigma_\kappa^{\mathrm{WKBJ}}(t_f) = \frac{\ln(G_\kappa^{\mathrm{WKBJ}}(t_f))}{t_f}. \tag{36}$$

As for a classical stability analysis, the most dangerous perturbations are expected to be the one which maximizes the above quantities. Thus, the most dangerous optimal initial wavenumber $\kappa^{\max}(t_f)$ is the initial wavenumber for which $\sigma_\kappa^{\max}(t_f)$ reaches its maximum

$$\sigma_{\max}^{\max}(t_f) = \max_{\kappa>0}\left[\sigma_\kappa^{\max}(t_f)\right]. \tag{37}$$

Similarly, the WKBJ approach provides a most dangerous initial wavenumber $\kappa^{\mathrm{WKBJ}}(t_f)$ and a maximum WKBJ mean growth rate $\sigma_{\max}^{\mathrm{WKBJ}}(t_f)$.

Contrarily to classical stability results, all the above quantities depend on the final (observation) time t_f. Moreover, as the system evolves in time, one has to keep in mind that the final characteristics of the system are a priori different from the initial ones. Formulas (8) and (9) tell us how the width and the velocity difference of the shear layer vary in time. They imply that the Reynolds number defined from these quantities varies from the initial Reynolds number Re_i according to

$$Re(t) = Re_i\frac{a(t)}{S(t)}. \tag{38}$$

The perturbation wavenumber is affected by the stretching field as demonstrated by expressions (12a) and (16). When non-dimensionalized by the shear layer width, it is therefore given by

$$k(t) = \kappa\frac{a(t)}{S(t)}, \tag{39}$$

where κ is the initial wavenumber. Note that these expressions for the Reynolds number and the wavenumber naturally appear in the local dispersion relation (33) of the WKBJ approach. It is also worth noticing that the combined effects of viscosity and stretching affect Reynolds number and wavenumber in a similar way. These two important parameters are both multiplied by a time-dependent factor $K(t) = a(t)/S(t)$. This "viscous-stretching factor" represents the kinematic effect of viscosity and stretching on the perturbation parameters. It tends to increase with viscosity and to decrease with stretching. As it will be shown in the following sections, most of the variations of the perturbations growth with respect to the parameters can be attributed to this kinematic effect. It is therefore important to provide its main characteristics.

Without stretching ($\gamma = 0$), the factor K increases in time as soon as viscosity is non-zero. On the contrary, when stretching is present ($\gamma(t) > c > 0$), $K(t)$ goes to zero for large time whatever the viscosity. There also exists a critical evolution $\gamma(t) = \gamma_c(t)$ for which $K(t)$ remains constant. It is given by

$$\gamma_c(t) = \frac{\nu}{1 + 2\nu t}. \tag{40}$$

In the following, the shear layer is usually assumed to be stretched with a constant positive stretching rate γ. In that case

$$K(t) = \exp(-2\gamma t)\sqrt{1 - 2\frac{\nu}{\gamma} + 2\frac{\nu}{\gamma}\exp(2\gamma t)}. \tag{41}$$

Fig. 1 illustrates the possible behaviors of K according to γ. If $\gamma > \nu$, $K(t)$ decreases for all t toward 0. One can say that stretching dominates over viscosity whatever t_f. If $\gamma < \nu$, $K(t)$ first increases up to a maximum value $K_{\max} = (\nu/\gamma)/\sqrt{2\nu/\gamma - 1}$, reached at $t_{\max} = \ln(2 - \gamma/\nu)/(2\gamma)$, and then decreases toward 0. It crosses the initial value $K = 1$ at $t_c = \ln(2\nu/\gamma - 1)/(2\gamma) = t_{\max} + \ln(\nu/\gamma)/(2\gamma)$. As long as $t_f < t_c$, it can be said that viscosity is dominant. For larger t_f ($t_f > t_c$), stretching takes over viscosity. This typical viscous-dominated then stretched-dominated evolution is indicated in dashed line on Fig. 1.

3. Optimal perturbations in an unstretched shear layer

Before analysing the effect of stretching on the stability properties of the shear layer, it is natural to fully understand the stability properties of the shear layer without stretching. In this section, we therefore determine the optimal perturbations of the shear layer in the case $\gamma = 0$. Two effects are analysed: the dependency with respect to the final time t_f and the effects of viscosity.

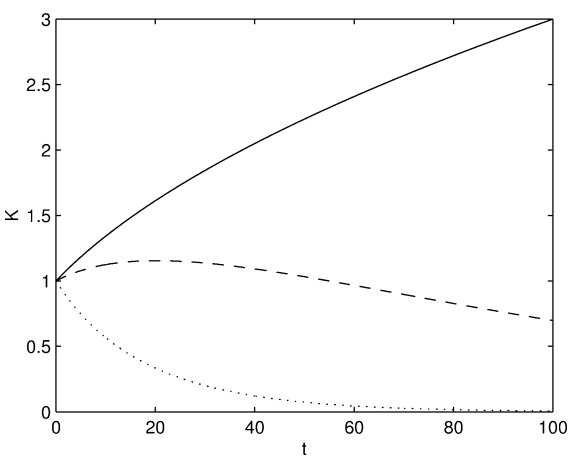

Fig. 1. Typical evolution of the viscous-stretching factor $K = a/S$ versus t (here for $Re = 50$). Solid line: viscous-dominated behavior ($\gamma = 0$). Dashed line: mixed viscous-stretched behavior ($\gamma = 0.01$). Dotted line: stretching-dominated behavior ($\gamma = 0.05$).

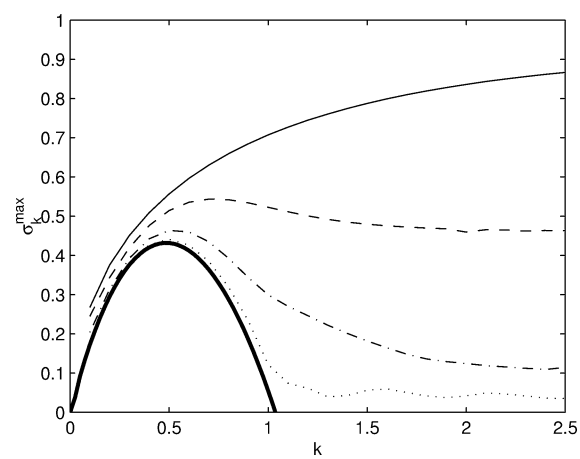

Fig. 2. Comparison of the non-viscous normal mode growth rate with the mean growth rate of the optimal perturbations for $Re = \infty$, $\gamma = 0$ and for various t_f. Thick solid line: non-viscous normal mode growth rate. Solid line: $t_f = 1$; dashed line: $t_f = 10$; dash-dot line: $t_f = 30$; dotted line: $t_f = 100$.

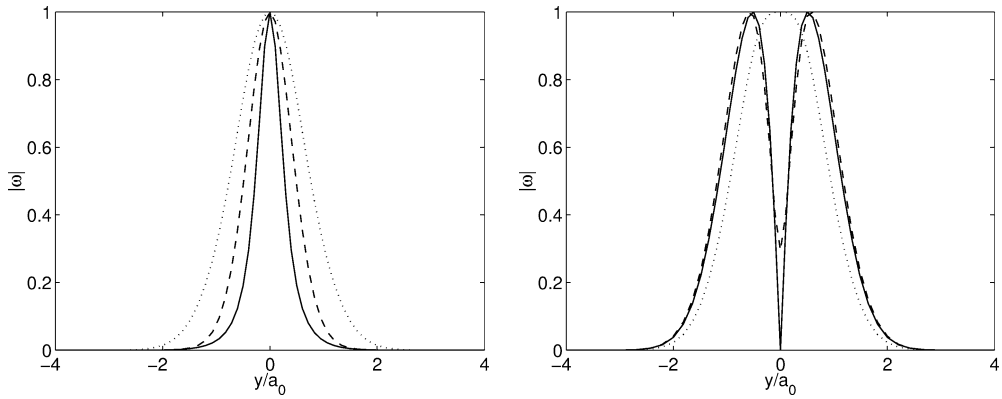

Fig. 3. Vorticity profiles of the optimal perturbations for $Re = \infty$, $\gamma = 0$, $\kappa = 0.5$ and various t_f. Dotted line: $t_f = 1$, dashed line: $t_f = 10$, solid line: $t_f = 100$. (a) Initial optimal perturbation (at $t = 0$). (b) Final optimal perturbation (at $t = t_f$). The solid lines also correspond to the profiles of the most unstable normal mode of the adjoint operator in (a), and of the direct operator in (b).

3.1. Non-viscous analysis

Transient effects associated with the non-normality of the evolution operator are best identified in the case $\nu = 0$ and $\gamma = 0$. In that case, no time-dependency is present in the coefficients of the perturbation equations: the above WKBJ analysis is therefore exact and reduces to a classical normal mode analysis. All the differences observed between WKBJ and optimal results can therefore be attributed to the non-modal character of the optimal perturbations.

Fig. 2 compares the non-viscous growth rate of the normal mode analysis with the mean growth rate of the optimal perturbation for various t_f. As expected, it is for the smallest t_f that the departure from the normal mode analysis is the strongest. For small t_f, optimal energy perturbations have large wavenumbers. For instance, for $t_f = 1$, the mean growth rate is maximum at $k \approx 17$. Progressively, as t_f increases, small wavenumbers become relatively more amplified. This is due to the Kelvin–Helmholtz instability. Unstable normal modes take over large wavenumber perturbations amplified during short transient when t_f becomes sufficiently large. Fig. 2 demonstrates that for $t_f = 100$, the stability characteristics of the optimal perturbation are strongly dominated by the unstable normal modes. It is also interesting to compare the vorticity profiles of the perturbations. Contrarily to normal mode analysis, optimal perturbation analysis provides two relevant perturbations: the initial perturbation (at $t = 0$) which is the perturbation one should make to maximize the gain, and the final perturbation (at $t = t_f$) which is the perturbation one should observe, and both depend on t_f. Initial and final optimal perturbation profiles (that is at $t = 0$, and $t = t_f$ respectively) are displayed on Fig. 3 (a) and (b) respectively. For large t_f, it is reassuring to see that, for the unstable wavenumber considered in Fig. 3, the final state of the optimal perturbation corresponds to the eigenmode of the normal mode analysis. The initial state is by contrast different whatever t_f. This is due to the non-self-adjoint nature of the evolution operator $\mathcal{L}_{\{\kappa,t\}}$ associated with the energy norm. However, for large t_f, the initial state converges toward the eigenmode of the adjoint operator, as expected from classical results (Schmid and Henningson [11]). The transient growth of large wavenumber for small times can be attributed to the so-called Orr mechanism (see, for instance, Schmid and Henningson [11]). This non-viscous mechanism is associated with the tilting of the disturbances into the direction of the mean shear and is known to cause an algebraic growth of the perturbation energy. This tilting phenomenon is illustrated on Fig. 4 (a) and (b) where are displayed the vorticity contours of the optimal perturbation at initial and final times for $t_f = 1$ and $\kappa = 8$.

3.2. Viscous analysis

Viscosity introduces two modifications. First, the normal mode properties of the shear layer are modified; second, the shear layer becomes time-dependent as its width evolves according to $a(t) = \sqrt{1 + 4\nu t}$. These two effects were first studied by Betchov and Szewczyk [5]. A physical interpretation in terms of time scales is also provided in Villermaux [26]. Betchov and Szewczyk [5] obtained the viscous normal modes numerically and considered the time-dependency of the basic flow using a WKBJ ansatz. They computed the perturbation gain between two instants thanks to a formula analogous to (35).

In this section, both effects are considered simultaneously using the optimization procedure. It is worth recalling that for O(1) Reynolds numbers, it is a priori the only suitable approach as the time-dependency of the basic flow forbids the normal mode decomposition used in the references cited above. Fig. 5 illustrates how the mean growth rate of the perturbation can be different according to the optimization procedure. Both the mean growth rate in the frozen basic flow and in the diffusing basic

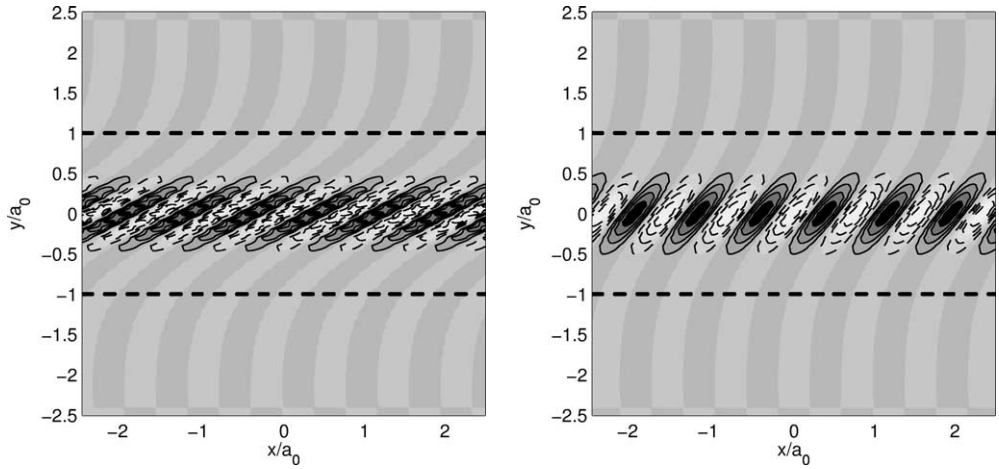

Fig. 4. Vorticity contours of the optimal perturbations in the (x, y) plane for $Re = \infty$, $\gamma = 0$, $\kappa = 8$, and $t_f = 1$. (a) Initial perturbation (at $t = 0$); (b) final perturbation (at $t = t_f$).

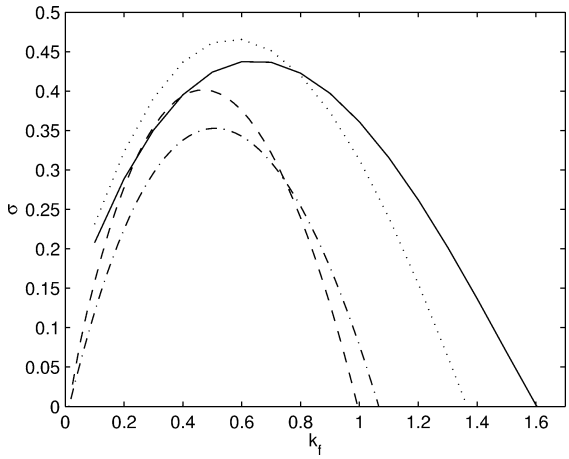

Fig. 5. Mean growth rate versus the final wavenumber k_f for $Re_i = 100$, $\gamma = 0$ and $t_f = 10$. Solid line: optimal perturbation. Dotted line: optimal perturbation in a frozen shear layer. Dash-dotted line: WKBJ perturbation. Dashed line: WKBJ perturbation in a frozen shear layer (viscous normal mode growth rate).

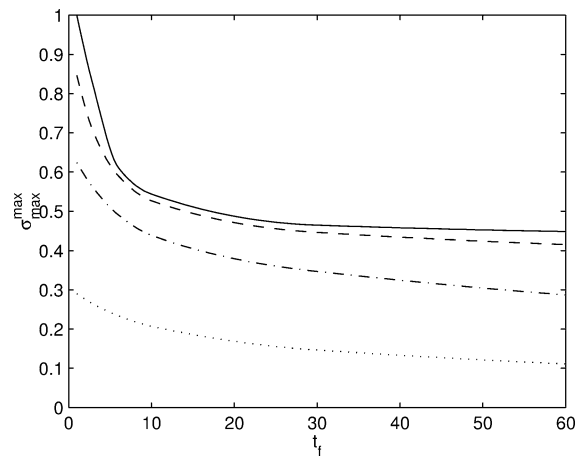

Fig. 6. Maximum mean growth rate of the optimal perturbations as a function of t_f for $\gamma = 0$. Solid line: $Re_i = \infty$; dashed line: $Re_i = 1000$; dash-dot line: $Re_i = 100$; dotted line: $Re_i = 10$.

flow are calculated by the energy optimization procedure and by the WKBJ approach. Two significant features are exhibited on this plot. (1) WKBJ approach underestimates the mean growth rate and the width of the amplified wavenumbers. (2) For both the WKBJ approach and the energy optimization procedure, the frozen basic flow possesses a larger maximum mean growth rate and a smaller most amplified wavenumber. The second point is a direct consequence from the fact that in the diffusing layer the final wavenumber has increased from the initial wavenumber by a factor equal to the final shear layer width $a(t_f) = \sqrt{1 + 4\nu t_f}$. On Fig. 6 is analysed the dependency of the maximum mean growth rate $\sigma_{\max}^{\max}$ with respect to the Reynolds number and the final optimization time t_f. The global stabilizing character of viscosity is clearly seen on this figure. Fig. 7 (a) and (b) display the most dangerous initial and final wavenumber of the optimal perturbation. The non-modal character of the optimal perturbation for small times is visible on this plot. Indeed, the wavenumber of the most dangerous optimal perturbation diverges as t_f goes to zero. This behavior is the signature of transient growth associated with the Orr mechanism. It cannot be due to an instability as all the normal modes are stable for $k > 1$. Note however that it is strongly weaken by viscosity. In particular, as soon as Re is smaller than 100, the wavenumber remains below 1.5 for $t_f = 1$ whereas one has $k_f^{\max} \approx 17$ for an infinite Reynolds number for the same final time. For larger times ($t_f > 10$), the most dangerous wavenumber varies much less with respect to

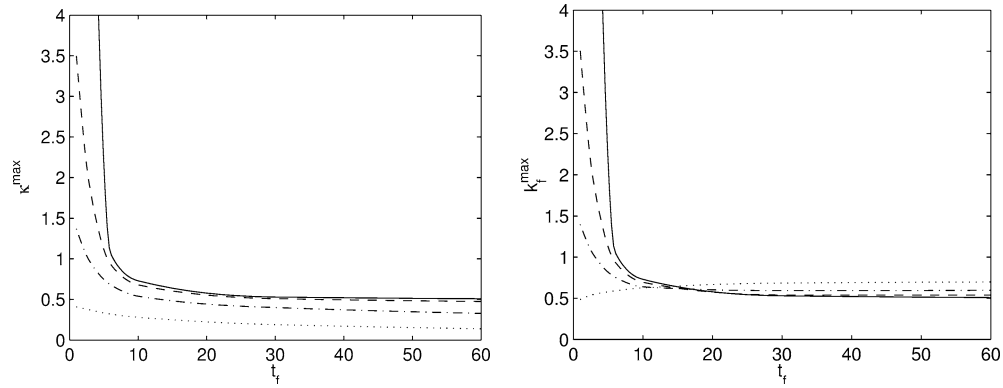

(a) (b)

Fig. 7. Initial wavenumber $\kappa^{\max}$ (a) and final wavenumber $k_f^{\max}$ (b) of the most dangerous optimal perturbation as a function of t_f for $\gamma = 0$. Solid line: $Re_i = \infty$; dashed line: $Re_i = 1000$; dash-dot line: $Re_i = 100$; dotted line: $Re_i = 10$.

time. The dynamics is no longer dominated by transient but by the instability. The initial wavenumber decreases slowly with t_f while the final optimal wavenumber is almost constant for $t_f > 10$. This constant depends slightly on the Reynolds number. It is approximatively $k_f^{\max} \approx 0.5$ for infinite Reynolds number and $k_f^{\max} \approx 0.7$ for $Re = 10$.

3.3. Comparison with Betchov and Szewczyk results

Using the WKBJ approach, Betchov and Szewczyk [5] calculated the energy gain between two instants t_1 and t_2 such that the local Reynolds number varies by a quantity $\Delta Re = Re_f - Re_i$. It is interesting to compare their results with the maximum gains obtained by the optimization procedure. With our normalization, $t_1 = 0$ and $t_2 = t_f$, one has $Re_i = 1/\nu$ and $Re_f = \sqrt{1 + 4\nu t_f}/\nu$, thus

$$t_f = \frac{(\nu \Delta Re + 1)^2 - 1}{4\nu}. \tag{42}$$

This formula clearly shows that t_f increases as the (initial) Reynolds number $Re_i = 1/\nu$ decreases. The smallest value $t_f = \Delta Re/2$ is obtained in the large Reynolds number limit. Fig. 8 displays for $\Delta Re = 30$, optimal energy gains and WKBJ gains for $Re_i = 10$ and $Re_i = \infty$ which correspond to $t_f = 37.5$, $t_f = 15$ respectively. The same features as those pointed out above are seen on these figures: WKBJ analysis underestimates the maximum gain, the value of the most dangerous wavenumber and the widths of the amplified wavenumbers.

Two WKBJ estimates are considered here. The dashed lines are the WKBJ estimates (35) as defined in Section 2.3.3 with $C^{\mathrm{WKBJ}} = 1$. The dotted lines are also WKBJ estimates but obtained by considering only the main behavior of the WKBJ approximation (that is the exponential factor) as it is done in Betchov and Szewczyk [5]. The ratio of the two estimates is a_f. For large Reynolds number, the two WKBJ estimates are equal: dotted curves and dashed curves superimpose for $Re_i = \infty$. For small Reynolds numbers, $a(t)$ varies significantly between $t = 0$ and $t = t_f$, so the two WKBJ estimates depart from each others. A priori, none of the two estimates is justified for small Reynolds numbers since the WKBJ approximation breaks down in this limit. However, the reduced WKBJ estimate seems to work better for small Reynolds numbers.

Note that there are some discrepancies between our WKBJ curves and those obtained by Betchov and Szewczyk [5]. For $Re_i = 0$ and $Re_i = \infty$, Betchov and Szewczyk obtained maximum gains of about 20 and 80 for final wavenumbers around $k_f \approx 0.5$ and $k_f \approx 0.75$ respectively. These gains are an order of magnitude smaller than ours and the most amplified final wavenumber increases with Re_i while in our case it decreases (see also Fig. 7(b)). We are confident in our results. Moreover, the fact that the most amplified wavenumber should be close to 0.5 (and not 0.75 as in Betchov and Szewczyk) for large Reynolds numbers is obvious since in this limit the WKBJ wave becomes a non-viscous normal mode for which the maximum growth rate is reached for $k = 0.5$.

Betchov and Szewczyk claimed that transition should occur when the Reynolds number has reached $Re_f = 150$, starting from $Re_i = 0$. They based their estimate on the so-called "e^N" which predicts a "natural" transition when the amplitude gain reaches e^9, that is an energy gain of order $e^{18} \approx 6.5 \times 10^7$. Based on our results, we expect such a factor to be obtained for smaller Reynolds numbers. Thus, transition should occur earlier. On Fig. 9 is plotted the contour levels of the energy gain in the $(Re_i, \Delta R)$ plane. The "transition level", indicated in dashed line, is reached for ΔRe between 75 and 110 depending on the initial Reynolds number. In the limit $Re_i \to 0$, the transition level is close to $\Delta Re \approx 110$.

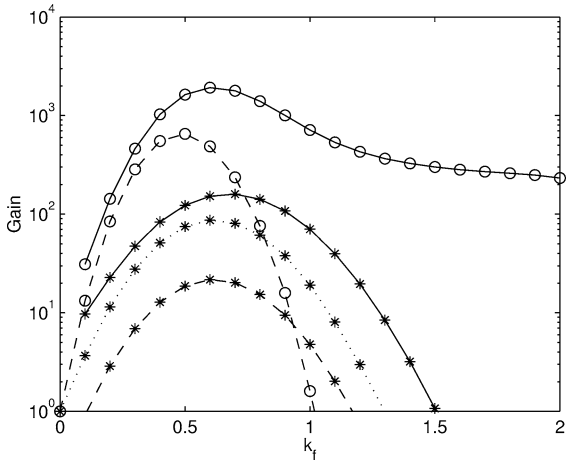

Fig. 8. Energy gain between Re_i and $Re_f = Re_i + 30$. Solid lines: optimal perturbation; dashed lines: WKBJ estimate; dotted line: reduced WKBJ estimate; stars: $Re_i = 10$; circles: $Re_i = \infty$.

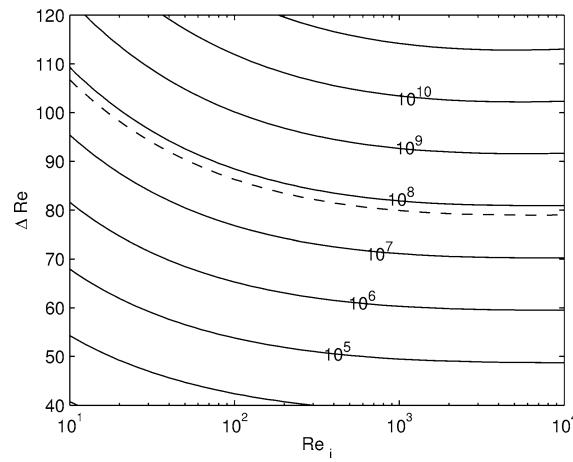

Fig. 9. Contour levels of the maximum energy gain in the $(Re_i, \Delta Re)$ plane. The dashed line is "e^{18}" energy level.

4. Optimal perturbations of a stretched shear layer

In the following sections, a stretching field is always present. As shown in Section 2.4, this field significantly affects the evolution of parameters such as the Reynolds number and the wavenumber. In presence of stretching, these parameters which follow the viscous-stretching factor $K(t)$ given in (41), always start to decrease if one waits sufficiently long. For this reason, stretching is always expected to have a dominant kinematic effect for large times whatever its (positive) value.

Moderate time intervals during which viscous and stretching effects are both present are considered in the first two subsections. We shall demonstrate that the main qualitative features of the evolution of the optimal energy gains with respect to stretching and viscosity can be associated with the variations of the viscous-stretching factor. Moreover, a precise quantitative comparison of the optimal results with the WKBJ estimates is also performed to identify the effect of stretching on the non-modal part of the optimal perturbations.

The perturbation evolution for large times is considered in a third subsection by asymptotic methods.

4.1. Stretching effects on the optimal perturbations

The results of the optimization procedure are summarized on Figs. 10(a)–(c). The maximum energy gain is plotted as a function of t_f in Fig. 10(a) for initial Reynolds numbers $Re_i = 100$ and $Re_i = 10000$ and stretching rates $\gamma = 0.001$ and $\gamma = 0.025$. For these values, initial and final wavenumbers of the most dangerous optimal perturbations are given in Fig. 10 (b) and (c) respectively. On these figures, note first that the maximum energy gain is not significantly affected by stretching contrarily to viscosity which clearly damps the perturbations. By contrast, stretching has an important effect on the optimal wavenumber, as it can be seen on Fig. 10 (b) and (c). In particular, stretching is demonstrated to strongly increase the optimal initial wavenumber and to decrease the final one. Fig. 10 (b) and (c) also show that this tendency is weaken by viscosity.

Anticipating the good agreement between optimal and WKBJ gains demonstrated in the next section, these features can be qualitatively understood in the WKBJ framework. For the Reynolds numbers we consider, the shape of local dispersion relation $\sigma_{\text{erf}}(k, Re)$ does not vary much. Its maximum $\sigma_m \approx 0.4$ is reached near $k_m \approx 0.5$. As the WKBJ gain is calculated by integrating the local growth rate, the maximum gain is thus obtained when the local growth rate remains the longest close to σ_m. In terms of wavenumbers, this means that $k(t)$ must stay the longest close to k_m. As the local wavenumber $k(t)$ varies between κ and $k_f = K(t_f)\kappa$, the values of κ and k_f are directly connected to the viscous-stretching factor $K(t_f)$ given by (41). When $K(t_f) \approx 1$, κ and k_m are expected to be both close to $k_m \approx 0.5$. This is indeed the case for $Re_i = 10000$ and $\gamma = 0.0001$. When $K(t_f)$ increases above 1 due to viscosity (for the case $Re_i = 100$ and $\gamma = 0.0001$ for instance), κ decreases below k_m and k_f increases above k_m, as expected. On the contrary, κ increases and k_f decreases when $K(t_f)$ decreases, as it is the case for the curves with $\gamma = 0.025$.

If one uses this argument for the gain, one would expect the maximum gain reached at a given time to be the largest when $K(t)$ is the closest to 1. In Fig. 10(a), this would be for $Re_i = 10000$ and $\gamma = 0.001$. This is actually not the case as the

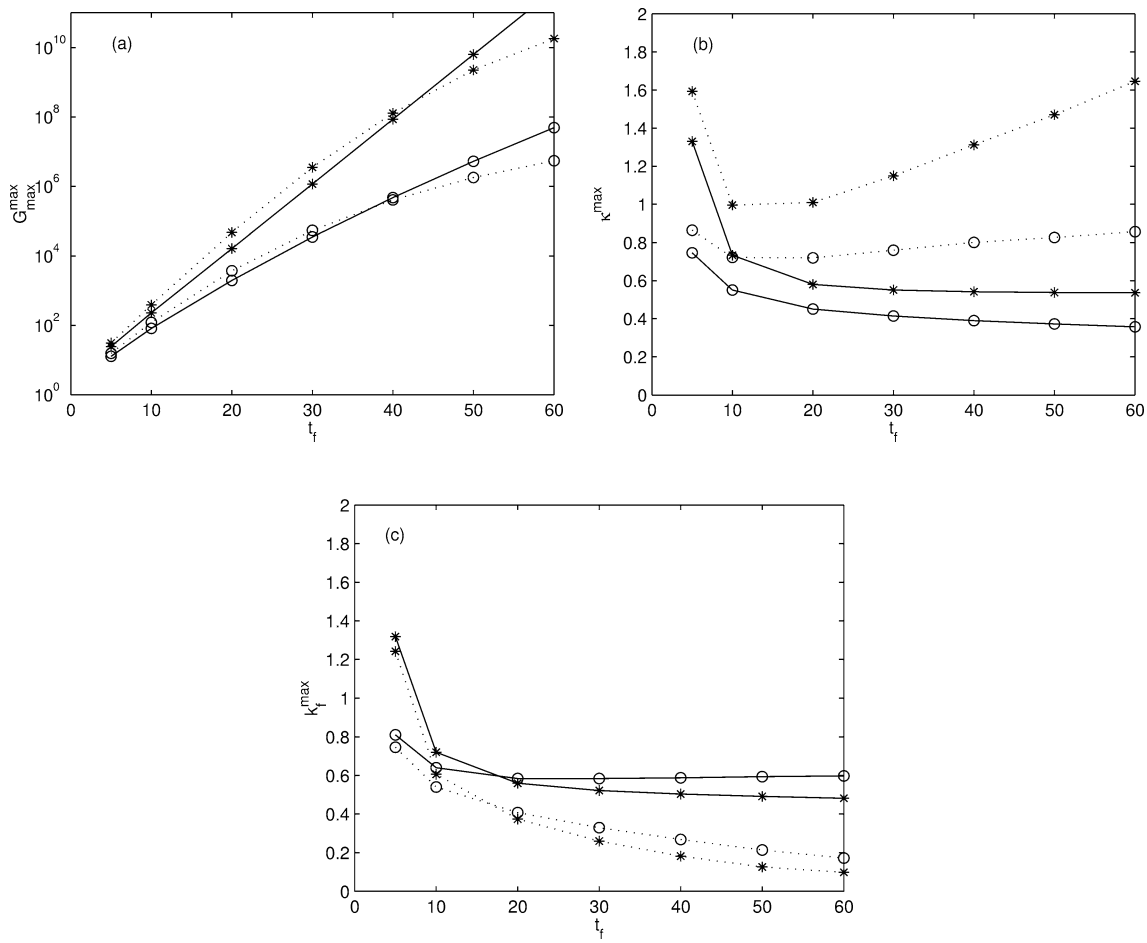

Fig. 10. Optimal perturbation characteristics versus t_f. (a) Maximum energy gain. (b) Initial optimal wavenumber. (c) Final optimal wavenumber. Solid lines: $\gamma = 0.001$; dotted lines: $\gamma = 0.025$. Symbols: $*$: $Re_i = 10000$; $\circ$: $Re_i = 100$.

parameters $Re_i = 10000$ and $\gamma = 0.025$ lead to a bigger gain for $t_f < 45$. The explanation could be related to the slowly-varying amplitude terms in front of the exponential in the WKBJ estimate (35). These terms are in particular associated with the time-decreasing behavior of the basic flow velocity. When stretching increases these terms increase as well. When $K(t)$ is not too small, they can be sufficiently large to compensate the fact that σ is not always close to its maximum.

A few features cannot be explained by the WKBJ approach. The first one is the characteristics for small t_f. Optimal wavenumbers increases as t_f goes to zero. This typical behavior is the signature of important transient growth for large wavenumbers. This has been seen in Section 3. It is associated with the non-viscous tilting mechanism (Orr mechanism) discussed in Section 3.1. It is reduced by viscosity but not significantly affected by stretching.

The second feature is the initial wavenumbers above 1 for large t_f in the case $Re_i = 10000$ and $\gamma = 0.025$. This is not expected by the quasi-static approach because the local normal mode are damped for wavenumbers larger than 1. The fact that these modes are selected is also reminiscent of the transient growth of large wavenumbers associated with the Orr mechanism.

Fig. 11 (a) and (b) provide the profiles of the vorticity norm of the optimal perturbation for two typical cases, dominated either by viscosity (a) or stretching (b). On each figure are plotted both the initial and the final vorticity profile obtained by the optimization procedure. The final profile is also compared to the profile of the most unstable local normal mode obtained for the final wavenumber $k_f^{\max}$. All the profiles have been normalized in amplitude by their maximum and the transverse coordinate by the width of the shear layer. Note first that optimal perturbation profiles are very similar to those obtained in Section 3.1 (Fig. 3) where neither stretching nor viscosity were present. The convergence of the final profile towards the local normal mode, observed in Section 3.1 is here also clear: the final optimal perturbation is almost indistinguishable from the local normal mode of same wavenumber. This evidence supports the assumption that we shall make in the analysis for large t in Section 4.3: for large t, the optimal perturbation becomes a single WKBJ mode.

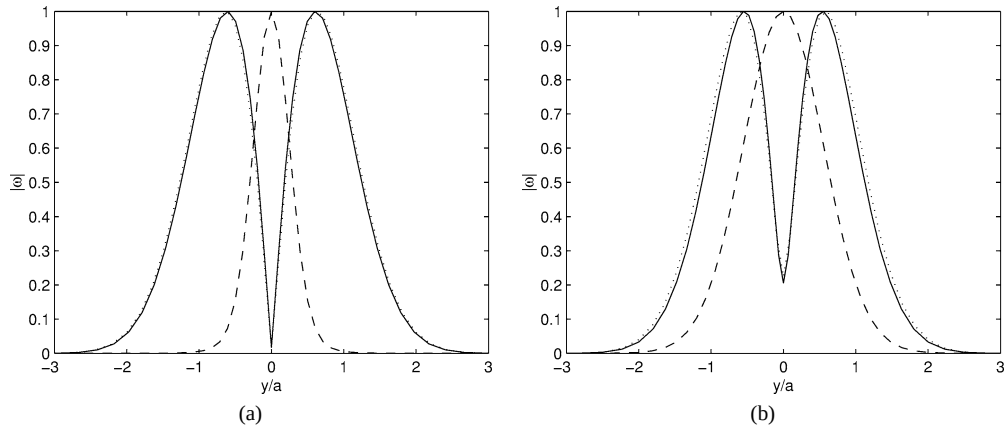

Fig. 11. Comparison of the perturbation vorticity profile $|\omega|$. Dashed lines: initial optimal perturbation (at $t = 0$). Solid lines: final optimal perturbation (at $t = t_f$). Dotted lines: WKBJ approximation for the final optimal wavenumber. (a) $Re_i = 10000$, $\gamma = 0.025$, $t_f = 30$. (b) $Re_i = 100$, $\gamma = 0.001$, $t_f = 30$.

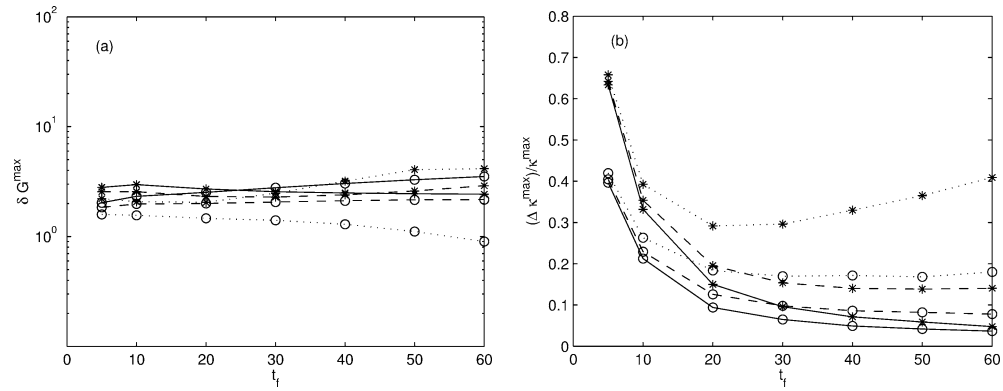

Fig. 12. Comparison of optimal and WKBJ results for various Re_i and γ. (a) Maximum gain ratio $\delta G^{\max} = G^{\max}_{\max}/G^{\mathrm{WKBJ}}_{\max}$. (b) Initial most dangerous wavenumber relative difference $\Delta\kappa^{\max}/\kappa^{\max} = 1 - \kappa^{\mathrm{WKBJ}}/\kappa^{\max}$. Solid lines: $\gamma = 0.001$; dashed lines: $\gamma = 0.01$; Dotted lines: $\gamma = 0.025$. Symbols: $*$: $Re_i = 10000$, $\circ$: $Re_i = 100$.

4.2. Quantitative comparison between optimal values and WKBJ estimates

The convergence of the optimal perturbation toward a single WKBJ mode as t_f increases could explain the good agreement between optimal and WKBJ gains shown on Fig. 12(a). On this figure is plotted versus t_f the ratio $\delta G^{\max} = G^{\max}_{\max}/G^{\mathrm{WKBJ}}_{\max}$ of the maximum optimal gain by the maximum WKBJ gain for several γ and Re_i. One can see that for all the cases studied, this ratio remains between 0.9 and 4. This is surprisingly close to 1, notably for the largest values of γ and t_f for which S is equal to 4.5 (for $\gamma = 0.025$ and $t_f = 60$). For such a large value of S, the factor C^{WKBJ} could be no longer close to 1. Note in particular, that if one would take the estimate $C^{\mathrm{WKBJ}} = 1/S^2$ obtained in Section 4.3 for large t and $Re = \infty$, one would get values for $\delta G^{\max}$ close to 70. Whatever the real expression of C^{WKBJ}, the closeness of the WKBJ estimate to the optimal gain proves that transient growth remains limited in terms of gain for all γ and Re_i. Differences are however visible on the characteristics of the optimal perturbation, as already mentioned above. Fig. 12(b) compares the most dangerous optimal wavenumber $\kappa^{\max}$ with the most dangerous WKBJ wavenumber κ^{WKBJ}. The relative difference $\Delta\kappa^{\max}/\kappa^{\max} = (\kappa^{\max} - \kappa^{\mathrm{WKBJ}})/\kappa^{\max}$ is plotted versus t_f for the same parameters as in Fig. 12(a). Except for the case of strong stretching and large Reynolds number, the relative difference decreases as time increases and becomes smaller than 20% for $t_f > 20$.

When t_f goes to zero, $\Delta\kappa^{\max}/\kappa^{\max}$ increases whatever the parameters. In this limit, as for the non-viscous unstretched case, the optimal wavenumber increases while the WKBJ wavenumber converges to the wavenumber of the most unstable normal mode. Note however this tendency is not significantly affected by stretching.

Interestingly, stretching effect becomes apparent only for large t_f, and all the more apparent, the Reynolds number is large. For instance, for very large Reynolds numbers ($Re_i > 10000$), $\Delta\kappa^{\max}/\kappa^{\max}$ increases with time although the optimal

gain converges toward the WKBJ estimate. Again, this behavior could be attributed to the kinematic effect of stretching if one assumes that the optimal perturbation in a stretched environment has, at each time t, a local growth rate which is approximatively given by the mean growth rate of the unstretched optimal perturbation at $t_f = t$ and for the same local wavenumber (that is given by the curves displayed in Fig. 2). Indeed, as γ increases, $K(t)$ decreases toward 0 and thus k covers a larger wavenumber interval during a given time period. As large wavenumbers ($k > 1$) possess large mean growth rates for small times (say $t < 10$), $\kappa^{\max}$ has to increase to keep the local wavenumber above 1 during a given small time interval (say $0 < t < 10$) in order to maximize the gain. In the meantime, κ^{WKBJ} remains in the unstable wavenumber range whatever t_f and is close to 1 for large t_f. This simple argument explains why $\Delta\kappa^{\max}/\kappa^{\max} = \Delta k_f^{\max}/k_f^{\max}$ increases with γ for very large Reynolds numbers.

4.3. Asymptotic analysis for small wavenumbers

Results of the previous sections have all shown energy gain increasing with the final optimization time t_f. It is thus natural to address the question whether this gain is unbounded as $t_f \to \infty$.

Moreover, we have seen in Section 4.1, that the final most dangerous optimal wavenumber decreases as t_f increases. This tendency has been attributed the kinematic effect of stretching, discussed in Section 2.4. Indeed, any wavenumber is multiplied during its time evolution by the viscous-stretching factor $K(t)$ which goes to zero as t_f goes to infinity. As soon as stretching is present, we therefore expect the final most dangerous wavenumber to go to zero for large t_f. Unfortunately, small wavenumbers cannot be easily resolved with our code which has a fixed grid. The difficulty comes from the inversion of the Poisson equation (17b) which becomes singular for small wavenumbers, its solution being non-localized. This difficulty precludes the use of our numerical code to analyse the large time limit. Insights can however be obtained from the previous sections. In Section 4.2, we have in particular shown that maximum optimal gain is well-estimated by the maximum WKBJ gain. Although discrepancies have been observed concerning the wavenumbers, the typical examples considered above in Fig. 11 (a) and (b) demonstrate that the spatial structure of the optimal perturbation is actually close to its WKBJ approximation for large t_f. In the limit of large t_f, it is therefore legitimate to assume that the optimal perturbation converges toward the WKBJ approximation of same local wavenumber.

As the optimal perturbation gets closer to the WKBJ approximation, the local wavenumber $k(t)$ decreases toward zero. The growth rate of the local normal mode thus also decreases. It eventually becomes $\mathrm{O}(\gamma)$ or $\mathrm{O}(\nu/\bar{a}^2)$ for sufficiently large time. When this occurs, the WKBJ approximation breaks down as there is no longer separation of time scales. A specific analysis has therefore to be performed to analyse the large time behavior of the perturbations.

In the appendix, such an analysis is carried out for the non-viscous case ($Re = \infty$). The final results of the asymptotic study are now presented.

When $k(t) = \kappa/S^2(t)$ becomes $\mathrm{O}(\gamma)$, an approximation for the streamfunction is given at leading order by (expression (A.15))

$$\psi_\kappa \sim \frac{c_0}{S^2(t)}\left(2\mathbf{K}_1\left(\frac{\kappa}{2\gamma S^2}\right) + \mathrm{i}\overline{U}_0(\bar{y})\mathbf{K}_0\left(\frac{\kappa}{2\gamma S^2}\right)\right), \tag{43}$$

where $\mathbf{K}_0$ and $\mathbf{K}_1$ are modified Bessel functions. The coefficient c_0 is a constant normalization factor. This approximation is obtained under the assumption that for earlier times, that is $k(t) \gg \gamma$, the solution is a single WKBJ mode (30). In (43), the stretching rate γ may depend on time as long as S is defined by expression (4).

From expression (43), an estimate for the energy density is obtained as (expression (A.17))

$$E_\kappa^{\mathrm{asym}} \sim E_\kappa^{(0)} \frac{|\mathbf{K}_0(\kappa/(2\gamma S^2))|^2}{S^2(t)},$$

where $E_\kappa^{(0)}$ is independent of time. The (relative) energy gain is therefore given by an expression of the form

$$G_k^{\mathrm{asym}} \sim G_\kappa^{(0)}\left|\mathbf{K}_0\left(\frac{\kappa}{2\gamma S^2}\right)\right|^2. \tag{44}$$

The behavior of the modified Bessel function $\mathbf{K}_0(x) \sim -\ln(x)$ near $x = 0$ implies that

$$G_\kappa^{\mathrm{asym}} \propto \ln\left[\gamma \exp\left(2\int_0^t \gamma(r)\,\mathrm{d}r\right)\right]^2 = \left(\ln\left(\gamma S^2\right)\right)^2. \tag{45}$$

For a constant positive stretching rate, the relative energy gain is therefore unbounded and grows linearly in time. This conclusion seems in contradiction with results obtained by Moore and Griffith-Jones [16] (see also Saffman [27]). They showed that an expanding circular vortex sheet is "stable" as soon as the radius $R/R_0 = S$ grows faster than t. Here, for a constant

stretching rate, S is exponentially growing, so the shear layer should be "stable". The apparent contradiction comes from the definition of stability used by Moore and Griffith-Jones [16]: they did not consider the evolution of the basic flow and assume stability as soon as the perturbation amplitude (or equivalently its energy) remains bounded. This is equivalent to base the stability criterion on the behavior of $E_\kappa^{\text{asym}}(t)$ instead of $G_\kappa^{\text{asym}}(t)$. We think that our definition is physically more relevant.

If one considers $E_\kappa^{\text{asym}}(t)$, it is easy to show that the results of Moore and Griffith-Jones [16] are recovered. In particular, for a constant stretching rate, $E_\kappa^{\text{asym}}(t)$ goes to zero for large times. In fact, the energy of the perturbation reaches its maximum for $\kappa/(2\gamma S^2) \approx 0.15$ and then decreases as $\kappa/(2\gamma S^2)$ becomes smaller. The unboundedness of the relative energy gain $G_\kappa^{\text{asym}}(t)$ obtained above is thus due to the fact that the energy of the basic flow decreases faster than that of the perturbation.

5. Discussion

5.1. Summary

In this paper, the evolution of two-dimensional linear perturbations to a stretched and viscous shear layer has been studied. The perturbations which maximize the relative energy gain during a given period of time $(0, t_f)$ have been computed for various parameters of the basic flow ($Re = 10 - \infty$; $\gamma = 0 - 0.025$) and optimization time ($t_f = 1 - 100$). The results have been compared to WKBJ estimates for which the perturbation is locally approximated by the most unstable local normal mode. The main conclusions are the following. Transients are visible for small times and favor large wavenumbers. They can be attributed to the tilting of the perturbation spatial structure into the mean shear direction as described by the so-called Orr mechanism. They are weaken by viscosity but not significantly affected by stretching. For larger times ($t_f > 10$), the final optimal perturbation (at $t = t_f$) is well-approximated by a single normal mode. The variations of the optimal perturbation characteristics are qualitatively well-described by the WKBJ approach. In this framework, the energy gain is roughly given by the integral of local normal mode growth rates during 0 ant t_f. During this time interval both the Reynolds number and the local wavenumber evolve according to the viscous-stretching factor $K = a/S = (1 + 4\nu \int_0^t S^2)^{1/2}/S^2$ with $S = \exp(\gamma t)$ which goes to zero in presence of stretching. The effects of stretching on the energy gain have been shown to be globally weak. Visible effects are mostly due to the variation of the local Reynolds number that stretching induces.

An asymptotic study has been performed for small wavenumbers and infinite Reynolds numbers in order to analyze the large time behavior of the perturbations. This study has shown that the energy gain is unbounded if the shear layer remains stretched. This divergence has been attributed to the stronger decay of the basic flow energy than of the perturbations.

5.2. Three-dimensional effects

The optimization procedure has been limited to two-dimensional perturbations. We have seen that modal growth due to the Kelvin–Helmholtz instability and non-modal growth associated with transients were in competition for small times. In 3D, we expect such a competition to be still present. Other sources of transient growth may however exist. Three-dimensional transient growth, such as the one associated with the so-called lift-up effect (see, for instance, Schmid and Henningson [11]), is known to provide important gains in boundary layer flows. Whether these effects become important in the shear layer remain an interesting open question for the future.

In the rest of the paper, we show that we can estimate the 3D growth associated with the instability by forming WKBJ estimates as in Section 2.3. For this purpose, we consider a more general basic flow in which a third component of the stretching field is present. This will permit to compare our results with Beronov and Kida [14] and Gomez and Rossi [15]. If one assumes that the basic flow vorticity is still Gaussian, the basic flow velocity field can be written as

$$\overline{U} = \big(U_0(y,t) + \gamma_x x, -(\gamma_x + \gamma_z)y, \gamma_z z\big), \tag{46}$$

where $U_0 = (1/S_x)\,\mathrm{erf}(y/a)$ and

$$a(t) = \frac{\sqrt{1 + 4\nu \int_0^t S_x^2 S_z^2}}{S_x S_z}, \qquad S_x(t) = \exp\left(\int_0^t \gamma_x\right), \qquad S_z(t) = \exp\left(\int_0^t \gamma_z\right).$$

The parameters γ_x and γ_z are the stretching rates in the principal directions Ox and Oz, respectively. The previous 2D basic flow is recovered when $\gamma_z = 0$.

If we follow the analysis of Section 2.3.3, a single 3D mode solution is obtained, for small γ_x, γ_z and ν, in the form

$$(\bar{u}, p) = (\bar{v}, q) \exp\left(\int_0^t \sigma\right) \exp(\mathrm{i}\kappa_x \bar{x} + \mathrm{i}\kappa_z \bar{z}) \tag{47}$$

with

$$\sigma = \frac{1}{aS_x}\sigma_{3D}\left(\frac{\kappa_x a}{S_x}, \frac{\kappa_z a}{S_z}, \frac{a}{\nu S_x}\right), \tag{48}$$

where $\sigma_{3D}(k_x, k_z, Re)$ is the 3D dispersion relation associated with the "erf" velocity profile. The main behaviour of the energy density is then

$$G_{3D}^{WKBJ} \approx \exp\left(2\int_0^t \sigma\right). \tag{49}$$

This expression can be compared to the 2D gain by the following manipulations. As it is well known, the 3D dispersion relation is connected to the dispersion relation of 2D perturbations by Squire's transformation (see, for instance, Drazin and Reid [2]):

$$\sigma_{3D}(k_x, k_z, Re) = \frac{k_x}{\sqrt{k_x^2 + k_z^2}}\sigma_{2D}\left(\sqrt{k_x^2 + k_z^2}, \frac{k_x}{\sqrt{k_x^2 + k_y^2}}Re\right).$$

Moreover, for the "erf" velocity profile, it is easy to check that $\sigma_{2D}(k, Re)/k$ is a function decreasing with respect to both k and $1/Re$ (this is also the case for a "tanh" profile (see Betchov and Szewczyk [5])). It follows that σ in (48) satisfies

$$\sigma \leqslant \frac{1}{aS_x}\sigma_{2D}\left(\frac{\kappa_x a}{S_x}, \frac{a^2\kappa_x}{\nu S_x^2\sqrt{(\kappa_x a/S_x)^2 + (\kappa_z a/S_z)^2}}\right) \leqslant \frac{1}{aS_x}\sigma_{2D}\left(\frac{\kappa_x a}{S_x}, \frac{a}{\nu S_x}\right).$$

If one applies the last inequality to (49), one obtains

$$G_{3D}^{WKBJ} \leqslant G_{2D}^{WKBJ}, \tag{50}$$

where G_{2D}^{WKBJ} is the main behaviour of the 2D gain (exponential factor in expression (35)). This inequality means that 3D perturbations provide less important gains than 2D perturbations whatever the stretching rates γ_x and γ_z.

The qualitative effect of spanwise stretching (along the vorticity direction Oz) can also be captured by the same type of consideration. For instance, in an inviscid flow, we have for two-dimensional perturbations (since $a = 1/(S_x S_z)$)

$$\sigma = S_z\sigma_{2D}\left(\frac{\kappa_x}{S_x^2 S_z}, \infty\right) \geqslant \sigma_{2D}\left(\frac{\kappa_x}{S_x^2}, \infty\right) \tag{51}$$

as soon as $S_z \geqslant 1$. The second term is the local growth rate of 2D perturbations without spanwise stretching. This inequality implies that spanwise stretching always increases the gain of 2D perturbations in an inviscid flow.

In presence of viscosity, we have the same conclusion as soon as

$$S_z \Big/ \sqrt{1 + 4\nu\int_0^t S_x^2 S_z^2} \geqslant 1 \Big/ \sqrt{1 + 4\nu\int_0^t S_x^2}$$

for all t. Since this is equivalent to

$$4\nu\left(S_z^2\int_0^t S_x^2 - \int_0^t S_x^2 S_z^2\right) + \left(S_z^2 - 1\right) \geqslant 1$$

which is automatically verified if S_z is an increasing function, spanwise stretching also favors the growth of 2D perturbations whatever the viscosity.

Note finally that spanwise compression has an opposite effect because all the above inequalities are reversed: the local growth rate in presence of spanwise compression is always smaller than the local growth rate of the mode with the same initial wavenumber without compression. Therefore, spanwise compression tends to stabilize the shear layer.

Recently, Gomez and Rossi [15] analysed the optimal energy perturbations of a discontinuous model of shear layer which is stretched in the spanwise direction only. They showed by computing the optimal perturbations that the energy gain grows when the spanwise stretching rate increases, and that it decreases in presence of compression. Their results are perfectly in agreement with our simple analysis based on the WKBJ approach.

Similarly, Beronov and Kida [14] showed that a Burgers layer for large Reynolds numbers was linearly less stable that the same shear layer without stretching. However, they also showed that this is not the case for very small Reynolds numbers as Burgers layer becomes linearly stable below $Re = 1$. The reason of this apparent discrepancy is explained in Beronov and

Kida [14]. The normal modes of the Burgers layer are strongly localised with a behavior for large $|y|$ which is independent on their local wavenumbers. This is not the case for the local normal modes of the same shear layer without stretching for which the behavior for large $|y|$ depends on the local wavenumber. In particular, for small k the local normal modes spread far away from the shear layer and tend to be non-localized when $k \to 0$. A WKBJ approach which is based on such modes cannot therefore describe the temporal stability characteristics of the stretched shear layer in that case.

Financial support by O.N.E.R.A. is gratefully acknowledged.

Appendix A. Small wavenumber asymptotic study for $Re = \infty$

In this section, an asymptotic study for small wavenumbers and infinite Reynolds number is performed. A weak stretching field is assumed to be present ($0 < \gamma \ll 1$) such that the local wavenumber given by $k(t) = \kappa/S^2$ always becomes small for large times. We assume that the perturbation has converged to the WKBJ approximation of the local most unstable mode before the breakdown of this approximation when $k(t)$ becomes of order γ. The goal of this section is to obtain a new approximation when $k(t) \leqslant \mathrm{O}(\gamma)$ in order to determine the behavior of the perturbation for very large times.

The framework is Eqs. (17a,b) with $\nu = 0$. If one introduces the new variables

$$\phi = S^2 \psi_\kappa, \tag{A.1a}$$

$$T = \kappa \int_0^t \frac{\mathrm{d}u}{S^2(u)}, \tag{A.1b}$$

Eqs. (17a,b) become for ϕ

$$\left(\frac{\partial}{\partial T} + \mathrm{i}\overline{U}_0\right)\left(\frac{\partial^2}{\partial \bar{y}^2} - \frac{\kappa^2}{S^4(t)}\right)\phi - \mathrm{i}\overline{U}_{0\bar{y}\bar{y}}\phi = 0. \tag{A.2}$$

For large $|\bar{y}|$, $\overline{U}_{0\bar{y}\bar{y}}$ is exponentially small, so ϕ must satisfy

$$\phi \sim \phi_{+\infty} \exp\left(-\frac{\kappa \bar{y}}{S^2}\right) \quad \text{when } \bar{y} \to +\infty, \tag{A.3a}$$

$$\phi \sim \phi_{-\infty} \exp\left(\frac{\kappa \bar{y}}{S^2}\right) \quad \text{when } \bar{y} \to -\infty. \tag{A.3b}$$

These conditions will be used to solve equation (A.2) in the bulk region ($|\bar{y}| = \mathrm{O}(1)$). As long as $|\bar{y}| = \mathrm{O}(1)$, the streamfunction ϕ can be expanded as

$$\phi = \phi_0 + \kappa/S^2 \phi_1 + \cdots \tag{A.4}$$

Eq. (A.2) becomes at leading order

$$\left(\frac{\partial}{\partial T} + \mathrm{i}\overline{U}_0\right)\frac{\partial^2 \phi_0}{\partial \bar{y}^2} - \mathrm{i}\overline{U}_{0\bar{y}\bar{y}}\phi_0 = 0. \tag{A.5}$$

Integrating this equation once with respect to $\bar{y}$ and writing

$$\phi_0 = \left(\frac{\partial}{\partial T} + \mathrm{i}\overline{U}_0\right)\mu_0 \tag{A.6}$$

leads to

$$\left(\frac{\partial}{\partial T} + \mathrm{i}\overline{U}_0\right)^2 \frac{\partial \mu_0}{\partial \bar{y}} = C_0(T).$$

An expression for the general solution of this equation can be obtained. However, conditions (A.3a,b) imply $C_0(T) = 0$. Moreover, we have assumed that the solution matches a WKBJ approximation for larger $k(t)$, that is when $T \to -\infty$. This condition implies that the streamfunction should decrease as $T \to -\infty$ which yields $\partial \mu_0/\partial \bar{y} = 0$. Thus μ_0 is a function of T only. This function is determined by solving the problem at the next order. Note however that the function μ_0 is connected to the functions $\phi_{+\infty}$ and $\phi_{-\infty}$ appearing in (A.3a,b) by the relations

$$\phi_{+\infty} = \left(\frac{\partial}{\partial T} + \mathrm{i}\right)\mu_0, \tag{A.7a}$$

$$\phi_{-\infty} = \left(\frac{\partial}{\partial T} - \mathrm{i}\right)\mu_0. \tag{A.7b}$$

The second order $(\kappa/S^2)\phi_1$ satisfies the same equation (A.5) as ϕ_0. Therefore, if

$$\phi_1 = S^2\left(\frac{\partial}{\partial T} + \mathrm{i}\overline{U}_0\right)\mu_1 \tag{A.8}$$

one has,

$$\left(\frac{\partial}{\partial T} + \mathrm{i}\overline{U}_0\right)^2 \frac{\partial \mu_1}{\partial \bar{y}} = C_1(T). \tag{A.9}$$

The matching of $\phi_0 + (\kappa/S^2)\phi_1$ with expressions (A.3a,b) for ϕ for large $|\bar{y}|$ requires that

$$\left.\frac{\partial \phi_1}{\partial \bar{y}}\right|_{\pm\infty} = \mp\phi_0|_{\pm\infty} = \mp\left(\frac{\partial}{\partial T} \pm \mathrm{i}\right)\mu_0. \tag{A.10}$$

This implies, using (A.8) and (A.9),

$$\mp\left(\frac{\partial}{\partial T} \pm \mathrm{i}\right)\frac{1}{S^2}\left(\frac{\partial}{\partial T} \pm \mathrm{i}\right)\mu_0 = C_1(T)$$

which leads, after eliminating $C_1(T)$, to an amplitude equation for μ_0

$$\left(\frac{\partial}{\partial T}\frac{1}{S^2}\frac{\partial}{\partial T} - \frac{1}{S^2}\right)\mu_0 = 0. \tag{A.11}$$

This equation can be easily integrated for any $\gamma = \gamma(t)$ by introducing the new variable

$$X = \frac{k}{2\gamma S^2}, \tag{A.12}$$

which transforms (A.11) into a modified Bessel equation:

$$\left(X^2\frac{\partial^2}{\partial X^2} + X\frac{\partial}{\partial X} - X^2\right)\mu_0 = 0. \tag{A.13}$$

Two independent solutions of this equation are the modified Bessel functions $\mathbf{I}_0(X)$ and $\mathbf{K}_0(X)$. The assumption that the solution should match the WKBJ approximation of an unstable growing mode for $T \to -\infty$, i.e., for large X, permits to exclude $\mathbf{I}_0(X)$ from the solution. The function $\mu_0(T)$ is then given by

$$\mu_0 = c_0\mathbf{K}_0(X), \tag{A.14}$$

where c_0 is a constant.

A leading order approximation for the streamfunction ψ_κ is then obtained from (A.1a), (A.4), (A.6), (A.12) and (A.14) as

$$\psi_\kappa \sim \frac{c_0}{S^2(t)}\left(2\mathbf{K}_1\left(\frac{\kappa}{2\gamma S^2}\right) + \mathrm{i}\overline{U}_0(\bar{y})\mathbf{K}_0\left(\frac{\kappa}{2\gamma S^2}\right)\right). \tag{A.15}$$

For large $\kappa/(\gamma S^2)$, this expression reads

$$\psi_\kappa \sim f_\kappa(\bar{y})\frac{\exp(-\kappa/(2\gamma S^2(t)))}{S(t)}.$$

One can check that it matches the WKBJ approximation (30) for small κ/S^2 and $Re = \infty$ provided that $F(t,k,\infty) \sim 1/S(t)$ as $k \to 0$.

A leading order expression for the vorticity ω_κ can also be derived from this expression by differentiating twice with respect to y:

$$\omega_\kappa \sim -\mathrm{i}c_0\overline{U}_{0\bar{y}\bar{y}}(\bar{y})\mathbf{K}_0\left(\frac{\kappa}{2\gamma S^2}\right). \tag{A.16}$$

From (A.15) and (A.16), one gets an estimate for the energy of the mode k using (22)

$$E_\kappa(t) \sim |c_0|^2 B\left(\int_{-\infty}^{+\infty} |\overline{U}_{0\bar{y}}|^2\right) \frac{|\mathbf{K}_0(\kappa/(2\gamma S^2))|^2}{S^2(t)}. \tag{A.17}$$

Note that similar expressions in terms of Bessel functions have been obtained by Moore and Griffith-Jones [16]. Their results were however obtained in a different framework where the shear layer was circular and infinitely thin (circular vortex sheet).

References

[1] L. Rayleigh, On the stability, or instability, of certain fluid motions, Proc. London Math. Soc. 11 (1880) 57–70.
[2] P.G. Drazin, W.H. Reid, Hydrodynamic Stability, Cambridge University Press, 1981.
[3] R.E. Esch, The instability of a shear layer between two parallel streams, J. Fluid Mech. 3 (1957) 289–303.
[4] T. Tatsumi, K. Gotoh, The stability of free boundary layers between two uniform streams, J. Fluid Mech. 7 (1960) 433–441.
[5] R. Betchov, A. Szewczyk, Stability of a shear layer between parallel streams, Phys. Fluids 6 (10) (1963) 1391–1396.
[6] C.-M. Ho, P. Huerre, Perturbed free shear layers, Annu. Rev. Fluid Mech. 16 (1984) 365–424.
[7] P. Huerre, P.A. Monkewitz, Absolute and convective instabilities in free shear layers, J. Fluid Mech. 159 (1985) 151–168.
[8] L.N. Trefethen, A.E. Trefethen, S.C. Reddy, T.A. Driscoll, Hydrodynamic stability without eigenvalues, Science 261 (1993) 578–584.
[9] K.M. Butler, B.F. Farrell, Three-dimensional optimal perturbations in viscous shear flow, Phys. Fluids A 4 (8) (1992) 1637–1650.
[10] B.F. Farrell, P.J. Ioannou, Generalized stability theory. Part I: Autonomous operators. Part II: Nonautonomous operators, J. Atmos. Sci. 53 (14) (1996) 2025–2053.
[11] P.J. Schmid, D.S. Henningson, Stability and Transition in Shear Flows, in: Appl. Math. Sci., Vol. 142, Springer, 2001.
[12] S.J. Lin, G.M. Corcos, The mixing layer: determistic models of a turbulent flow. Part 3: The effect of plane strain on the dynamics of streamwise vortices, J. Fluid Mech. 141 (1984) 139–178.
[13] J.C. Neu, The dynamics of stretched vortices, J. Fluid Mech. 143 (1984) 253–276.
[14] K.N. Beronov, S. Kida, Linear two-dimensional stability of a burgers vortex layer, Phys. Fluids 8 (1996) 1024–1035.
[15] T. Gomez, M. Rossi, Instabilité d'une nappe de vorticité étirée instationnaire, C. R. Acad. Sci. Paris 331 (2003) 141–147.
[16] D.W. Moore, R. Griffith-Jones, The stability of an expanding circular vortex sheet, Mathematika 21 (1974) 128–133.
[17] D.W. Moore, The stability of an evolving two-dimensional vortex sheet, Mathematika 23 (1976) 35–44.
[18] P. Luchini, A. Bottaro, Görtler vortices: a backward-in-time approach to the receptivity problem, J. Fluid Mech. 363 (1998) 1–23.
[19] P. Andersson, M. Berggren, D.S. Henningson, Optimal disturbances and bypass transition in boundary layers, Phys. Fluids 11 (1) (1999) 134–150.
[20] G.-H. Cottet, P.D. Koumoutsakos, Vortex Methods: Theory and Applications, Cambridge University Press, Cambridge, 2000.
[21] G.K. Batchelor, An Introduction to Fluid Dynamics, Cambridge University Press, Cambridge, 1967.
[22] K.N. Beronov, Vorticity layers in unbounded viscous flow with uniform rates of strain, Fluid Dynamics Res. 21 (1997) 285–302.
[23] R.W. Melcalfe, S.A. Orszag, M.E. Brachet, S. Menon, J.J. Riley, Secondary instability of a temporally growing mixing layer, J. Fluid Mech. 184 (1987) 207–243.
[24] J.A.C. Weideman, S.C. Reddy, A matlab differentiation matrix suite, ACM T. Math. Software 26 (4) (2000) 465–519.
[25] M. Van Dyke, Perturbation Method in Fluid Mechanics, The Parabolic Press, Stanford, 1975.
[26] E. Villermaux, On the role of viscosity in shear instabilities, Phys. Fluids 10 (2) (1998) 368–373.
[27] P.G. Saffman, Vortex Dynamics, Cambridge University Press, 1992.